HHS Public Access

Author manuscript

Mol Pharm. Author manuscript; available in PMC 2018 May 01.

Published in final edited form as:

Mol Pharm. 2017 May 01; 14(5): 1418–1428. doi:10.1021/acs.molpharmaceut.7b00045.

Pharmacokinetic and biodistribution studies of HPMA copolymer conjugates in an aseptic implant loosening mouse model

Xin Wei[1], **Fei Li**[1], **Gang Zhao**[1], **Yashpal Singh Chhonker**[1], **Christine Averill**[2], **Josselyn Galdamez**[2], **P. Edward Purdue**[2], **Xiaoyan Wang**[1], **Edward V. Fehringer**[3], **Kevin L. Garvin**[3], **Steven R. Goldring**[2], **Yazen Alnouti**[1], and **Dong Wang**[1,3,*]

[1]Department of Pharmaceutical Sciences, University of Nebraska Medical Center, Omaha, NE, 68198, USA

[2]Hospital for Special Surgery, New York, NY, 10021, USA

[3]Department of Orthopaedic Surgery and Rehabilitation, University of Nebraska Medical Center, Omaha, NE, 68198, USA

Abstract

N-(2-Hydroxypropyl) methacrylamide (HPMA) copolymers were previously found to represent a versatile delivery platform for the early detection and intervention of orthopedic implant loosening. In this manuscript, we evaluated the impact of different structural parameters of the HPMA copolymeric system (e.g. molecular weight (MW), drug content) to its pharmacokinetics and biodistribution (PK/BD) profile. Using ^{125}I, Alexa Fluor® 488 and IRDye® 800 CW-labeled HPMA copolymer-dexamethasone (P-Dex) conjugates with different MW and dexamethasone (Dex) contents, we found the MW to be the predominant impact factor on the PK/BD profiles of P-Dex, with Dex content as a secondary impact factor. In gamma counter-based PK/BD studies, increased MW of P-Dex reduced elimination, leading to lower clearance, longer half-life, and higher systemic exposure (AUC and MRT). In the semi-quantitative live animal optical imaging evaluation, the distribution of P-Dex to the peri-implant inflammatory lesion increased when MW was increased. This result was further confirmed by FACS analyses of cells isolated from peri-implant regions after systemic administration of Alexa Fluor® 488-labeled P-Dex. Since the *in vitro* cell culture study suggested that the internalization of P-Dex by macrophages is generally independent of P-Dex' MW and Dex content, the impact of the MW and Dex content on its PK/BD profile was most likely exerted at physiological and pathophysiological levels rather than at the cellular level. In both gamma counter-based PK/BD analyses and semi-quantitative optical imaging analyses, P-Dex with 6 wt% Dex content showed fast clearance. Dynamic light scattering analyses unexpectedly revealed significant molecular aggregation of P-Dex at this Dex content level. The underlining mechanisms of the aggregation and fast *in vivo* clearance of the P-Dex warrant further investigation.

*Correspondence should be addressed to Dong Wang, Department of Pharmaceutical Sciences, University of Nebraska Medical Center, 986125 Nebraska Medical Center, PDD 3020, Omaha, NE 68198-6125. Phone: 402-559-1995. Fax: 402-559-9543. dwang@unmc.edu.

Graphical Abstract

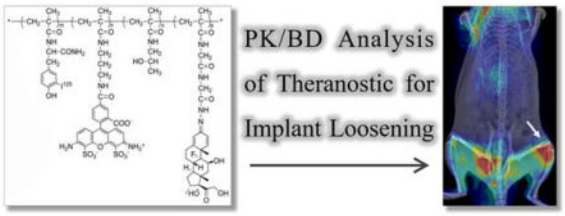

Keywords

Pharmacokinetics; Biodistribution; HPMA copolymer; Inflammation targeting; Dexamethasone; Implant loosening; ELVIS

1. Introduction

Aseptic implant loosening triggered by orthopedic implant wear particles is well recognized as the main cause of prosthetic failure after arthroplasty.[1–3] Peri-prosthetic osteolysis can be detected by radiographic techniques, such as CT, planar X-ray or MRI, as the pathology develops.[4, 5] Unfortunately, when the peri-implant osteolysis is radiographically confirmed, the condition is mostly irreversible, leaving revision surgery as the only treatment option which is more expensive, and often associated with poorer clinical outcomes.[6–8] Currently there is no US FDA approved therapeutic intervention for aseptic implant loosening. Furthermore, no early diagnostic tool is available to report the cascade of biological events preceding the radiographic detection of osteolytic lesions, making the timing for any potential therapeutic intervention unpredictable.

Recently, we have explored the potential utility of *N*-(2-Hydroxypropyl) methacrylamide (HPMA) copolymer conjugates as a theranostic platform for early diagnosis and prophylactic treatment of peri-prosthetic osteolysis.[9, 10] Because of the nature of this synthetic, water-soluble polymer-based theranostic platform, structural parameters (such as average molecular weight (MW), drug loading, and the presence of active targeting ligands) are all known to have significant impact on the platform's *in vivo* pharmacokinetic and biodistribution (PK/BD) profile. In addition, the pathophysiology features (e.g. inflammation) may have a profound impact on the platform's *in vivo* fate. HPMA copolymer conjugates' PK/BD profiles have been characterized in multiple animal models of human diseases.[11–14] In this manuscript, we will focus on elucidating the impact of different structural parameters on HPMA copolymer conjugates' PK/BD profile in an aseptic orthopedic implant loosening mouse model. The results from this study will help identify the optimal structural design of the HPMA copolymer-based theranostic platform for early diagnosis and prophylactic treatment of peri-prosthetic osteolysis, respectively.

2. Material and methods

2.1. Materials

N-(2-Hydroxypropyl)methacrylamide (HPMA), *N*-methacryloylglycylglycylhydrazinyl dexamethasone (MA-Dex), *N*-methacryloyl tyrosinamide (MA-Tyr-NH_2) and *S,S′*-bis(α,α′-dimethyl-α″-acetic acid)-trithiocarbonate (CTA, purity >97%) were prepared as reported previously.[15] Sephadex LH-20 resin and PD-10 columns were obtained from GE HealthCare (Piscataway, NJ). The $Na^{125}I$ was purchased from Perkin-Elmer (Waltham, MA). IRDye® 800CW NHS ester was purchased from LI-COR, Inc (Lincoln, NE). Alexa Fluor® 488 NHS ester was purchased from Life Technologies (Eugene, OR). All other reagents and solvents were purchased from either Sigma-Aldrich (St. Louis, MO) or Acros Organics (Morris Plains, NJ). All compounds were reagent grade or higher and used without further purification.

Ten-week-old male CD 1® IGS mice were purchased from Charles River Laboratories and maintained under standard housing conditions. All animal experiments were performed in accordance with protocols evaluated and approved by the Institutional Animal Care and Use Committee (IACUC) of the University of Nebraska Medical Center.

2.2. Instruments

^1H and ^{13}C NMR spectra were recorded on a 500 MHz NMR spectrometer (Varian, Palo Alto, CA). A lambda 10 UV/Vis Spectrometer (PerkinElmer, Waltham, MA) was used for UV/Vis spectrophotometric analyses. A ÄKTA Fast Protein Liquid Chromatography system (FPLC, GE Healthcare Bio-Sciences, Pittsburgh, PA) equipped with Superdex 200 column, UV and RI (KNAUER, Berlin, Germany) detectors was used for analyses of P-Dex molecular weight. HPLC analyses were performed on an Agilent 1100 HPLC system (Agilent Technologies, Inc., Santa Clara, CA) with a reverse phase C_{18} column (Agilent, 4.6×250 mm, 5 μm). Zetasizer Nano ZS90 (Malvern, Worcestershire, UK) was used in P-Dex aggregation analyses. Isoflurane vaporizer (Midmark Corp, Dayton, OH) was used to anesthetize animals during live imaging analyses. A Faxitron® MX-20 Cabinet X-ray System (Faxitron Bioptics, Tucson, AZ) was used in the implant loosening model establishment to confirm the implant position. A Packard Cobra II Gamma Counter (PerkinElmer, Waltham, MA) was used in the tissue radioactivity counting in the gamma counter-based PK/BD study. A Pearl® Impulse small animal imaging system (LI-COR, Lincoln, NE) was used for near infrared (NIR) optical imaging of live animals. Flow cytometry on disaggregated cells was performed on a BD™ LSR II flow cytometer (BD Biosciences, San Jose, CA), and on BD FACS Scan and BD FACS Canto cytometers for the *in vitro* uptake studies.

2.3. Synthesis of ^{125}I-labeled HPMA copolymer-dexamethasone conjugates (P-Dex-^{125}I, Figure 1)

The HPMA copolymer-dexamethasone conjugates were synthesized by a reversible addition-fragmentation chain transfer (RAFT) copolymerization as described previously.[16] *N*-(2-Hydroxypropyl) methacrylamide (HPMA), *N*-methacryloyl glycylglycylhydrazyl dexamethasone (MA-Dex), *N*-methacryloyl tyrosine amide (MA-Tyr-NH_2) were dissolved

in anhydrous methanol and then copolymerized under argon at 45 °C for 48 hr with 2,2″-azobisisobutyronitrile (AIBN) as an initiator and *S,S*′-bis(α, α′-dimethyl-α″-acetic acid) trithiocarbonate (CTA) as the RAFT agent. The ratio of AIBN and CTA was adjusted to obtain HPMA copolymer-dexamethasone conjugates (P-Dex) with different molecular weight and the dexamethasone (Dex) content was regulated by adjusting the MA-Dex feed-in ratio. The final tyrosine amide-containing HPMA copolymer-Dex conjugates (P-Dex-Tyr-NH_2) were obtained by lyophilization after the removal of the unreacted low molecular weight compounds using LH-20 column.

To label the P-Dex-Tyr-NH_2 with ^{125}I, the tyrosine-containing copolymers (~ 1 mg) were dissolved in saline (50 μL, 0.9%) in a glass vial (1 mL). NaI^{125} solution (pH = 12, 20 μL, 1 mCi) and chloramine-T (100 μL, 4.8 mg/mL, saline) were sequentially added to the solution. This reaction was stirred at room temperature (0.5 hr) and quenched by $Na_2S_2O_3$ (6 mg/mL, in 100 μL saline). After purification by PD-10 column, twice, the resulting solution (1.5 mL) was obtained with strong radioactivity (~0.08–0.12 mCi). The entire labeling process was done according to a protocol approved by the University of Nebraska Medical Center Radiation Safety Office in a fume hood with face velocity of 100 FPM, and with lead shield protection. Post-labeling cleaning and contamination survey were performed to ensure the absence of any radiation contamination in the working area.

2.4. Synthesis of IRDye® 800CW-labeled P-Dex (P-Dex-IRDye, Figure 1)

P-Dex-APMA (the copolymers of HPMA and *N*-(3-aminopropyl) methacrylamide[10], 50 mg, containing ~0.0037 mmol of amine), IRDye® 800CW NHS ester (1.25 mg, 0.001075 mmol LI-COR® Biosciences, Lincoln, NE) were dissolved in dimethylformamide (DMF, 900 μL) with 15 μL of *N,N*-diisopropylethylamine (DIPEA) added. The solution was stirred overnight in darkness at room temperature. The product was then purified on an LH-20 column and lyophilized. The IRDye® 800CW content was determined using Lambda 10 UV/Vis Spectrometer.

2.5. Synthesis of Alexa Fluor® 488 labeled P-Dex (P-Dex-Alexa, Figure 1)

P-Dex-APMA (50.0 mg, containing ~0.0037 mmol of amine), Alexa Fluor® 488 NHS ester (0.75 mg, 0.001 mmol, Life Technologies, Eugene, OR) dissolved in DMF (900 μL) with DIPEA (15 μL) added. The mixture was stirred overnight in darkness at room temperature. The product was then purified on an LH-20 column and lyophilized. The Alexa Fluor® 488 content was determined using a Lambda 10 UV/Vis spectrometer.

2.6. Characterization of the HPMA copolymer conjugates

Size exclusion chromatography (SEC) with a ÄKTA fast protein liquid chromatography (FPLC) system was used to determine the number average molecular weight (M_n), weight average molecular weight (M_w) and the polydispersity index (PDI) of the copolymers using a calibration of HPMA homopolymers with narrow PDI. To quantify Dex content in P-Dex, the copolymers were hydrolyzed in 0.1 N HCl (1 mg/mL) overnight. The resulting solution was neutralized and analyzed on an Agilent 1100 high performance liquid chromatography (HPLC) system with a reverse phase C_{18} column (Agilent, 4.6 × 250 mm, 5 μm). Mobile phase, acetonitrile/water 2/3; detection, UV 240 nm; flow rate, 1 mL/min; injection volume,

10 μL. The analyses were performed in triplicate. The mean value and standard deviation were obtained using Excel. The characterizations of all HPMA copolymer conjugates used in this study are summarized in Table 1 and Table 2. The potential aggregation of the P-Dex (6 wt%) was characterized by DLS with a series of concentrations. Three measurements at each concentration were performed and the results were averaged and summarized in Table 7.

2.7. Establishment of a murine prosthesis failure model

A murine prosthesis failure model was established surgically as we described previously.[9] Poly(methyl methacrylate) (PMMA) particles (1–10 μm, Bangs Laboratories, Fishers, IN) were used to induce the peri-prosthetic inflammation. The position of the implant was validated with Faxitron® MX-20 Cabinet X-ray System. Mice were administrated antibiotics (cefazolin sodium, 20 mg/kg, s.c.) immediately after surgery and analgesics (buprenorphine, 0.5 mg/kg, s.c.) were given twice daily for three days after surgery. Biweekly intraarticular injection of PMMA particles (1 mg in 10 μL sterile saline) into the left knee joint was done postoperatively to mimic the gradual particle releasing process in the patients. Saline of similar volume was injected into the right knee as the control. A total of 180 male CD 1® IGS mice were used in the gamma counter-based PK/BD analysis experiment, and 25 mice were used for the NIR imaging-based PK/BD analysis.

2.8. Gamma counter-based pharmacokinetic and biodistribution analysis

On 30th day post implant introduction, ^{125}I-labeled and unlabeled P-Dex-Tyr-NH_2 conjugates (~1.5 μCi/mice, 5 mg polymer/mice) were mixed and administered to mice (5 mice/group) via tail vein injection. Animals were sacrificed at designated time points (0.5, 2, 6, 16, 48, 168 hr). Blood and other major organs/tissues including, heart, lungs, kidneys, liver, spleen, and both hind limbs were isolated at euthanasia. They were processed, and analyzed using a Packard Cobra II Gamma Counter without perfusion.

The pharmacokinetic parameters, such as total clearance (CL), the volume of distribution (V_d), and biological half-life ($t_{1/2}$) were determined using the bolus intravenous input non-compartmental analysis of WinNonlin (version 6.3, Pharsight, Mountain View, CA). The area under the curve (AUC) was calculated using the trapezoidal rule. The relative exposure ratio was calculated by dividing AUC_{tissue} by AUC_{blood}. AUC_{last} from both tissues and blood was used for the relative exposure ratio.

2.9. Near-infrared optical imaging analysis

On the 30th day post implant introduction, mice were given P-Dex-IRDye (0.3 mg/mice) via tail vein injection (5 mice/group). The mice were imaged at designated time points (0.5, 24, 48, 72, 96, 120, 144, 168 hr) using a Pearl® Impulse small animal imaging system to evaluate the distribution and retention of the IRDye-labeled prodrug. All mice were anesthetized with 2 % isoflurane throughout procedures and dehaired before imaging. Imaging acquisition condition is dual channel (800 nm and white light) with 85 μm resolution. Images for each mouse were normalized using the same intensity scale with a common minimum and maximum value. The signal intensity from the left joints were semi-quantitatively analyzed by the resident software (Pearl Impulse Software). The regions of

interest (ROI) with identical areas were selected manually as a 59×59 (pixels) ellipse shape using a drawing tool in the software at both knee joints and background (Figure 2). The center of the ROI was located to the knee joint. Signal intensity of the knee joint minus background signal intensity was then corrected for the area (pixels). Although the fluorescence dye content was controlled similar when synthesis, to compare with the signals from animals receiving different conjugates, a signal standardization method was developed as following: conjugate solutions (20 μL, 3 mg/mL) were dropped on a Petri dish and imaged at the same imaging conditions (Figure 2. A). The signals from the droplets were analyzed using the same method described above. The signal from the left knee joint was corrected according to the signal intensity obtained from conjugates droplets images in Figure 2.A in order to eliminate the impact of different dye content in the conjugates during the *in vivo* imaging analysis. The equation is listed below:

$$Standardized\ Mean\ Signal\ Intensity\ (\%) = \frac{I_L - I_B}{\frac{I_i - I_{Bi}}{20\mu L \times 3mg/mL} \times 0.3mg} \times 100\%$$

I_L: Mean signal intensity from left knee ROI

I_B: Mean signal intensity from background

I_i: Mean signal intensity from initial droplet

I_{Bi}: Mean signal intensity from background in initial droplet image

2.10. Fluorescence-Activated Cell Scanning (FACS) Analysis

The FACS analysis procedure was adapted from previous work.[10] Two days after the last intraarticular particle injection, the mice were given P-Dex-Alexa 488 (5 mg/mouse) via tail vein injection. At necropsy (24 hr post injection), the left femurs were isolated and minced aseptically. The tissues were further digested with type IA collagenase (1 mg/mL, Sigma-Aldrich) at 37 °C for 30 min twice. After passing through a 70 μm cell strainer, ACK Lysing Buffer (Quality Biological, Gaithersburg, MD) was then used to remove the red blood cells. After centrifugation (1200 rpm, 5 min), a single cell suspension (1×10^6 cells/50 μL) was obtained. For FACS evaluation of dendritic cells, macrophage, monocytes and fibroblast cells, the samples were incubated with the following antibodies: hamster anti-mouse CD11c (BD Biosciences, Pharmingen), Allophycocyanin (APC)-labeled rat anti-mouse F4/80 (eBioscience, San Diego, CA), APC-labeled rat anti-mouse Ly-6G (Gr-1, Gr1) (eBioscience, San Diego, CA) and Alexa Fluro® 647 labeled rabbit anti-mouse P4HB (Abcam, Cambridge, MA), respectively for 30 minutes on ice. Cells incubated with hamster anti-mouse CD11c were further treated with Alexa Fluro® 647-labeled goat anti-hamster secondary antibody for another 30 minutes on ice. All the cells were then fixed in FACS fixation buffer and stored at 4 °C prior to analyses on a BD™ LSR II flow cytometer.

2.11. *In vitro* Internalization Study of HPMA Copolymer Conjugates in Macrophages

To evaluate the internalization of HPMA copolymer conjugates *in vitro*, fluorescence microscopy and flow cytometry were used to conduct these studies:

Fluorescence microscope imaging: Primary BMMs were prepared by conventional procedures and plated onto glass coverslips at a density of 2.5×10^5 cells per well of a 12-well plate in alpha-MEM medium supplemented with 10% fetal bovine serum and 25 ng/mL M-CSF. After overnight incubation, copolymers were added from a 20 mg/mL stock in PBS to a final concentration of 40 μg/mL. After additional 24 or 48 hrs incubation, cells were washed with HBSS, labeled with Hoechst 33342 (2 μg/mL for 5 minutes in HBSS), fixed with 2% paraformaldehyde for 15 minutes at 37°C, washed with HBSS and mounted using ProLong Gold Antifade mounting medium. Cells were imaged and captured images were analyzed using a Nikon Eclipse fluorescence microscope.

Flow cytometric analysis: Primary BMMs were prepared by conventional procedures and plated in alpha-MEM medium supplemented with 10% FBS and 25 ng/mL M-CSF in petri dishes (one million cells in 8 mL per dish). After overnight incubation, polymers were added from a 20 mg/mL stock in PBS to a final concentration of 40 μg/mL. After additional incubation 4–48 hr, cells were washed with PBS, trypsinized, washed and resuspended in 0.6 mL stain buffer (BD Pharmigen). Cells were stained with a 7-AAD viability stain prior to flow cytometric analysis on FACScan or FACScanto cytometers.

2.12. Statistical Analysis

Differences in cell internalization and organ distributions of different HPMA copolymer conjugates were analyzed using one-way ANOVA. When differences were detected, Tukey's test was used to evaluate the pairwise differences between the groups.

3. Results

3.1. Characterization of HPMA Copolymer Conjugates

The synthesis of all the HPMA copolymer-dexamethasone conjugates and their labeling with ^{125}I and fluorescent labels were straightforward.[16] By employing RAFT copolymerization, we were able to control the MW of the HPMA copolymer conjugates and manage their PDI in a narrow range as shown in Tables 1 & 2. For *in vivo* studies, these conjugates were divided into two groups: the first group had similar Dex contents of ~12 wt % but differed in MW (ranging from ~15 kDa to ~45 kDa, M_w), and the second group had similar MW of ~30 kDa (M_w) but differed in Dex content (0 wt%, ~6 wt%, ~12 wt%). All copolymer conjugates contained a small amount of tyrosine amide to allow their ^{125}I labeling, and a similar amount of APMA providing the pendent primary amine for IRDye 800CW or Alexa 488 labeling.

3.2. The pharmacokinetics and biodistribution of the HPMA copolymer conjugates in the peri-implant osteolysis mouse model

3.2.1. Gamma counter-based PK/BD analyses of HPMA copolymer conjugates in the peri-implant osteolysis mouse model using ^{125}I-labled conjugates—The percentage of injected conjugates dose per gram (ID/g) of tissue vs. time (0.5, 2, 6, 16, 48, 168 hr post-injection) in all major organs, blood and both femurs are shown in Figure 3. For P-Dex with different MWs but the same Dex content (~12 wt%), MW clearly had a major impact on the distribution of P-Dex conjugates in major organs. Of all the conjugates tested,

P-Dex-40 kDa-12%, which has the highest MW, showed the maximum ID/g value in most of the organs examined at the earliest time points. In the kidney, however, the conjugate with the lowest MW (P-Dex-20 kDa-12%) was found with the highest ID/g values at the end point. While all other conjugates examined exhibited a biphasic clearance pattern, P-Dex-40 kDa-12%'s clearance showed a unique pattern. Increased ID/g values were found for P-Dex-40 kDa-12% during 2–6 hr post-injection in all tissue and organs, during 16–48 hr in the liver and both femurs, and during 48–168 hr in the spleen. Increased ID/g values were also found in both femurs and spleen during 2–6 hr post-injection with P-Dex-30kDa-0%. In all organs and tissues, P-Dex-30 kDa-6% showed the lowest ID/g at every time point. The difference between the PMMA particle-injected left femur and non-particle-injected right femur were not significant with all of the tested polymer conjugates, which is contrary to our previous findings.[17]

3.2.2. Biodistribution of HPMA copolymer conjugates in tissues according to the live optical imaging—Due to the insensitivity of gamma counter-based PK/BD analysis techniques in defining the differential distribution pattern of P-Dex conjugates between the femur with peri-implant osteolysis and the control, we performed additional analyses using P-Dex conjugates labeled with IRDye® 800CW. As shown in Figure 4, this approach confirmed the critical role of MW in determining the PK/BD profile. The retention time of the P-Dex *in vivo* increased with an increase in MW. Unlike the gamma counter-based PK/BD study, live NIR optical imaging permitted discrimination of the peri-implant inflammation site from the control site. The fluorescent signal intensity from left knee (with implant and particle infusion) increased with the increase of MW at the same time point post i.v. administration. When the signal from the knee joint was corrected as described in the equation in the method section, the semi-quantitative results (Figure 6) corroborate well with the visual observation. In Figure 5, the P-Dex-30 kDa-6% showed an unexpected PK/BD profile, comparing with all the other groups. The fast elimination of the conjugate was evidenced by the low signal from the mice after 48-hr post-injection. This result was in agreement with the gamma counter-based PK/BD experiment finding using P-Dex-^{125}I.

3.3. Gamma Counter-Based Pharmacokinetic Analyses

PK parameters of the tested conjugates in blood and major organs/tissues were obtained using a non-compartmental analysis (Table 3). Systemic exposure as expressed by AUC and MRT increased with increasing MW. For example, AUC of P-Dex-40 kDa-12% was ~26 fold higher than P-Dex-20 kDa-12%. Both V_d and Cl decreased with increasing MW, but the decrease in Cl was more pronounced, which lead to the overall increase in exposure as measured by AUC and MRT. Also the low Cl associated with higher MW formulation (P-Dex-40 kDa-12%) led to the longer half-life of 35.8 hr. Increasing the MW increased exposure of blood, as well as all other tissues as measured by AUC and MRT. Dex loading also affected the MRT and AUC. For example, P-Dex-30 kDa-0% had ~3-fold higher $AUC_{0\text{-}\infty}$ than P-Dex-30 kDa-6% and Cl of P-Dex-30 kDa-6% was ~3-fold higher than P-Dex-30 kDa-0%. While P-Dex-30 kDa-12% had ~2-fold higher $AUC_{0\text{-}\infty}$ than P-Dex-30 kDa-6% and Cl of P-Dex-30 kDa-6% was 2-fold higher than P-Dex-30 kDa-12%.

3.4. *In vivo* Fluorescence-Activated Cell Scanning (FACS) Analysis

For all the tested cell phenotypes ($CD11c^+$, $F4/80^+$, Ly-6G (Gr-1, Gr1)$^+$ and $P4HB^+$, see Figure 7), the percentage of cells that internalized the P-Dex copolymers increased with the increase of the MW of the polymers (e.g. P-Dex-15kDa-12%, P-Dex-35kDa-12% and P-Dex-45kDa-12%). This increase was highly significant when the MW was raised from 15 to 35 kDa. For instance, the percentage of CD11c positive cell increased from 41.67% to 89.28% when treated with P-Dex-15kDa-12% and P-Dex-35kDa-12%, respectively. The difference in the percentage of the cells that internalized the polymers was not significant, however, when MW was raised from 35 to 45 kDa. The Dex content also affected the cell uptake of P-Dex copolymers. With the increase of Dex content, the percentage of the cells that internalized the P-Dex copolymers was also increased for several of the cell phenotypes tested in this study (see Table 4).

As shown in Figure 8, over 90% of the cell-sequestered P-Dex-Alexa were found in Ly-6G (Gr-1, Gr1) positive cells. The cell uptake efficiency increased with the increases of P-Dex MW. The impact of the Dex content has on cell internalization efficiency was more complex. For example, more P-Dex with higher Dex content was sequestrated by F4/80 positive cell, while more P-Dex with lower Dex content was sequestered by Ly-6G (Gr-1, Gr1) positive cells (see Table 5).

3.5. The Impact of Structural Parameters on *In vitro* BMM Internalization P-Dex

To determine the effect of MW on cellular uptake of the HPMA copolymer conjugates, murine BMMs were incubated with Alexa-488 labeled P-Dex with Dex content ~12 wt% and different MW (ranging from 15 kDa to 45 kDa). Cells were analyzed using flow cytometry and fluorescence microscopy at 4, 24 and 48 hrs after addition of the copolymers to the cells. The flow cytometric data (Figure 9) revealed that all four of these copolymers were taken up by the BMMs, being detectable at 4 hrs and increasing throughout the time course. MW did not appear to have any significant effects on copolymer uptake, since the kinetics and levels of uptake were very similar between the four copolymers.

To determine the effect of Dex content on uptake of HPMA copolymers by BMMs, three copolymers of the similar MW (~35 kDa), but differing Dex content were analyzed by flow cytometry and fluorescence microscopy as described above. Flow cytometry revealed that the kinetics and levels of uptake of the P-Dex 35 kDa-6 wt% and P-Dex 35 kDa-12 wt% conjugates were indistinguishable (Figure 10 and Figure 11). Uptake of the dexamethasone-free copolymer appeared somewhat higher than that of the dexamethasone-containing copolymers, which may in part be due to the relatively higher loading of Alexa Fluor® 488 on this copolymer.

3.6. Dynamic Light Scattering Analysis of P-Dex

The dynamic light scattering analysis results of different P-Dex copolymers are presented in Table 6 and results for P-Dex-35 kDa-6% at different concentration can be seen in Table 7. The DLS data clearly suggest that P-Dex-35 kDa-6% forms aggregates under the conditions tested. This finding may partially explain the unexpected fast clearance of P-Dex-35 kDa-6% found in the PK/BD study.

4. Discussion

The passive targeting of nanomedicines, including water-soluble macromolecules after systemic administration has been validated in multiple animal models of inflammatory diseases, which encompass chronic systemic autoimmune disorders (e.g. rheumatoid arthritis, systemic lupus), acute local injuries (e.g. fracture) and chronic local inflammatory conditions (e.g. peri-implant osteolysis).[16, 18–20] We posited that the mechanism for this passive targeting is different from the Enhanced Permeability and Retention (EPR) Effect[21] and may be explained by an ELVIS mechanism (Extravasation through Leaky Vasculature and Inflammatory cell-mediated Sequestration)[22–24], in which the systemically administered nanomedicine would extravasate through the leaky vasculature at the inflammatory lesion and be sequestered locally via inflammatory cell infiltrates and activated resident cell. Concurrently, for systemic inflammatory conditions, a fraction of the nanomedicine administered may also be sequestered by white blood cells (WBC) in the circulation and be actively transported to the inflammatory lesion. Previously, we have found that the HPMA copolymers' structural parameters, such as average MW and drug loading have a significant impact on their pharmacokinetic and biodistribution (PK/BD) profile in a systemic inflammatory arthritis rat model.[13]

The focus of the present study, therefore, is to define the impact of MW and drug loading on PK/BD profile of HPMA copolymer-dexamethasone conjugates in a model of localized inflammation. For this purpose, we synthesized a series of HPMA copolymers with different MW or Dex content as described above. Using both ^{125}I-labeling/gamma counter techniques and the NIR optical imaging, we validated the impact of MW and Dex content on the PK/BD profiles of HPMA copolymers in the mouse model of aseptic implant loosening.

The Impact of molecular weight on PK/BD profile: MW clearly had a major impact on the PK/BD profiles of P-Dex conjugates in the gamma counter-based analyses (Figure 3). There was greater uptake and retention of the conjugates with the higher MWs in the major organs at every time point evaluated, with the kidney as the only exception, which may be due to the fact that the HPMA copolymer conjugates are known to be cleared through the kidney and the lower MW conjugates would be expected to have more rapid renal clearance.[25–27] This was also reported in our previous finding when analyzing the PK/BD profile of HPMA copolymer conjugates using inflammatory arthritis rat model.[13] The %ID/g of most of the P-Dex conjugates in all the organs and tissues decreased over time. In this analysis, we also found the ^{125}I activity (representing the amount of P-Dex) between the particle-injected left femur and non-particle-injected right femur was not significantly different, which was not consistent with our previous findings.[17, 28] The systemic exposure of the conjugate increased when the MW was raised. The $AUC_{0\text{-}\infty}$ (blood) of the conjugates positively correlated with the MW of the conjugates and Cl of the polymers was negatively correlated to the MW of the polymers. There is no significant difference between $AUC_{\text{left femur}}/AUC_{\text{bood}}$ and $AUC_{\text{right femur}}/AUC_{\text{bood}}$ for all the tested polymer conjugates. Review of the protocol suggests that the discrepancy may be attributed to the technical limitation of not being able to isolate the peri-implant inflammatory tissue from the surrounding noninvolved tissues. Instead, the whole leg was isolated without perfusion.

Since the tissue samples harvested were much larger than the peri-implant inflammatory lesion in this model, the radioactivity associated with the large quantities of non-relevant tissue may have masked the small activity of the P-Dex-^{125}I targeted to the peri-implant lesion, leading to the inconclusive results.

In order to overcome the limitation of the gamma counter-based PK/BD analyses, we conducted a semi-quantitative near-infrared optical imaging-based PK/BD analysis to better recapitulate the passive targeting of P-Dex to the peri-implant lesion. The methodology was successful in establishing the preferential localization of the P-Dex in the particle-injected left femurs and this was true for all the polymer conjugates tested. Furthermore, as evident in Figures 4 & 6, the increase of MW provided longer retention of the polymers at the peri-implant inflammatory site and better differentiation of the left (with particle infusion) and right (without particle infusion) legs. Also shown in Figure 6, there was a trend of increase of ROI signal intensity at 1-day post-injection for both P-Dex-35 kDa-12% and P-Dex-45 kDa-12% groups. This may be due to re-circulation of the copolymers in the system.[29]

The impact of drug loading on the PK/BD profile: Based on the findings presented in Figures 3, 5 and Table 3, higher Dex content provided a higher systemic exposure and a longer retention conjugates at the inflammatory site. An unexpected finding was that the P-Dex with ~ 6 wt% Dex content exhibited unusually rapid elimination in both gamma counter analysis and NIR optical imaging studies which was not found in our previous work using inflammatory arthritis rat model.[13] This experiment was repeated multiple times and the results were confirmed. Further examination revealed that the PBS or DD water solution of P-Dex-30 kDa-6% and P-Dex-35 kDa-6% was cloudy, which suggested the potential of polymer aggregation in the solutions. DLS analyses of the P-Dex-35kDa-6% in DD water confirmed the presence of aggregates and the aggregation size was positively correlated with the increase of the concentration. Compared to none-aggregating HPMA copolymers, the P-Dex-35kDa-6% aggregates (> 150 nm even after dilution associated with systemic administration) may be more rapidly internalized by the mononuclear phagocytic system (MPS), leading to their enhanced clearance.[30] The gamma counter-based PK/BD analysis, however, did not find high radioactivity in livers or spleens after P-Dex-35kDa-6% administration. The NIR optical imaging (Figure 5) seemed to support a very rapid renal clearance for the polymer. Clearly, the further investigations are necessary to better understand the mechanism of the copolymers aggregation and its rapid *in vivo* clearance.

To understand the impact of the P-Dex with different structural parameters on cell uptake and sequestration *in vitro*, BMMs were treated with P-Dex of different MW and Dex content and analyzed at different time points for copolymer uptake and sequestration by flow cytometry and fluorescence microscopy. The results of these experiments revealed no significant differences in the kinetics or levels of uptake between P-Dex of different MW or Dex content (which correlates with the finding of others),[31] suggesting that cell autonomous mechanisms for copolymer uptake and sequestration operate independently of MW or Dex content. To explore cellular uptake in the peri-implant tissue *in vivo*, Alexa Fluor® 488 labeled copolymers were given to mice. As shown in Figure 7, 8 and Table 4, 5, the FACS analysis of the peri-implant tissue confirmed that all the copolymers were predominantly taken up by inflammatory myeloid cells (including inflammatory monocytes, macrophages

and dendritic cells), with a minor component internalized by fibroblastic cells. For all cell populations analyzed, there was a trend towards increased frequencies of cells internalizing copolymer with increasing MW. In addition, the increase of Dex content also enhanced the cell-mediated sequestration, especially for the CD11c+ cells. Since our *in vitro* cell culture study suggested that the alteration of MW and Dex content would have minimal impact on BMM internalization of the P-Dex, we speculate that the increased *in vivo* sequestration of P-Dex with higher MW polymers and/or higher Dex content might be mainly attributed to their increased exposure to the cells as demonstrated by their higher $t_{1/2}$, AUC, MRT and lower Cl.

The results from this comprehensive study are informative in assisting the future structural design of HPMA copolymer-based theranostic system for early detection and prophylactic intervention of peri-implant osteolysis. Based on the findings of this study, we believe the use of a high MW (less than 45 kDa to ensure eventual renal clearance) HPMA copolymer as the carrier for MRI, SPECT/CT or PET/CT imaging modalities may provide the best early diagnostic tool. While this high MW would also cause the imaging probe's distribution to off-target anatomical locations, its potential risk of off-target toxicity is minimal due to its infrequent use and relatively low dosing level. For therapeutic intervention, the data from the current study also suggest that the use of a high MW (but less than 45 kDa to ensure eventual renal clearance) HPMA copolymer as the drug carrier to ensure the optimal targeting to the peri-implant inflammatory lesion. The off-target distribution and associated toxicities, however, cannot be underestimated in this case. While our previous study suggest the long-term use of P-Dex in managing peri-implant osteolysis may not cause systemic osteopenia[18], its impact on other sensitive organs and tissues (e.g. adrenal gland) is yet to be evaluated. If the safety profile of the HPMA copolymer-drug conjugate is not acceptable, a localized delivery strategy may be considered as an alternative. Though the mechanism is not yet understood, the finding of P-Dex aggregation at certain Dex content (6 wt%) must be carefully evaluated when considering clinical translation of this potential macromolecular prodrug conjugate, in order to ensure safety and a favorable PK/BD profile.

5. Conclusion

Using gamma counter-based and optical imaging-based methodologies, we evaluated the impact of structural parameters (i.e. molecular weight and drug content) on the pharmacokinetic and biodistribution (PK/BD) profiles of HPMA copolymer-dexamethasone conjugates in an aseptic peri-implant inflammation/osteolysis mouse model. The study found that the increase of both the MW and Dex content facilitated targeting of P-Dex to sites of local inflammation through increasing systemic exposure and reduced renal clearance of the conjugates. At certain level of Dex content (6 wt %), P-Dex may aggregate, leading to a more rapid elimination of the copolymers from the system. Our findings will assist in the future design and development of HPMA copolymer-based theranostic platform for early detection and therapeutic intervention of peri-implant osteolysis and implant failure.

Acknowledgments

This study was supported in part by the National Institute of Arthritis and Musculoskeletal and Skin Diseases of the National Institute of Health of the United States of America (R01AR062680) and the University of Nebraska Medical Center College of Pharmacy. The content is solely the responsibility of the authors and does not necessarily represent the official views of the National Institutes of Health.

Abbreviations

AIBN	2,2′-azobisisobutyronitrile
AUC	Area under the concentration-time curve
AUC_{blood}	Area under the concentration-time curve in plasma
AUC_{last}	Area under the concentration-time curve up to the last measurable concentration
AUC_{tissue}	Area under the concentration-time curve in soft tissues
BMM	Bone marrow derived macrophage
CL	Total clearance
CTA	Chain transfer agent
Dex	Dexamethasone
DLS	Dynamic light scattering
ELVIS	Extravasation through Leaky Vasculature and Inflammatory cell-mediated Sequestration
FACS	Fluorescence-activated cell scanning
FDA	Food and Drug Administration
FPLC	Fast protein liquid chromatography
HPLC	High performance liquid chromatography
HPMA	*N*-(2-Hydroxypropyl) methacrylamide
IACUC	Institutional Animal Care and Use Committee
ID/g	Injected dose per gram of tissue isolated
MA-Dex	*N*-Methacryloyl glycylglycylhydrazyl dexamethasone
MA-Tyr-NH_2	*N*-Methacryloyl tyrosine amide
M_n	Number average molecular weight
MPS	Mononuclear phagocytic system
MRI	Magnetic resonance imaging

MW	Molecular weight
M_w	Weight average molecular weight
NIR	Near-infrared
P-Dex	HPMA copolymer-dexamethasone conjugate
P-Dex-Alexa	Alexa Fluor® 488-labeled HPMA copolymer-dexamethasone conjugate
P-Dex-IRDye	IRDye® 800 CW-labeled HPMA copolymer-dexamethasone conjugate
P-Dex-APMA	Copolymers of HPMA and *N*-(3-aminopropyl) methacrylamide
PK/BD	Pharmacokinetics and biodistribution
PMMA	Poly(methyl methacrylate)
RAFT	Reversible addition-fragmentation chain transfer
ROI	Regions of interest
$t_{1/2}$	Half-life
V_d	Volume of distribution

References

1. Beaulé PE, Campbell PA, Walker PS, Schmalzried TP, Dorey FJ, Blunn GW, Bell CJ, Yahia LH, Amstutz HC. Polyethylene wear characteristics in vivo and in a knee stimulator. J Biomed Mater Res. 2002; 60(3):411–419. [PubMed: 11920665]
2. De Baets T, Waelput W, Bellemans J. Analysis of third body particles generated during total knee arthroplasty: Is metal debris an issue? The Knee. 2008; 15(2):95–97. [PubMed: 18255297]
3. Bal BS, Garino J, Ries M, Oonishi H. Ceramic bearings in total knee arthroplasty. J Knee Surg. 2007; 20(4):261–270. [PubMed: 17993065]
4. Talbot BS, Weinberg EP. MR Imaging with Metal-suppression Sequences for Evaluation of Total Joint Arthroplasty. Radiographics. 2016; 36(1):209–225. [PubMed: 26587889]
5. Obert L, Peyron C, Boyer E, Menu G, Loisel F, Aubry S. CT scan evaluation of glenoid bone and pectoralis major tendon: interest in shoulder prosthesis. SICOT-J. 2016; 2:33. [PubMed: 27716461]
6. Brown J, Mistry J, Cherian J, Elmallah R, Chughtai M, Harwin S, Mont M. Femoral Component Revision of Total Hip Arthroplasty. Orthopedics. 2016; 39(6):e1129–e1139. [PubMed: 27575035]
7. Vulcano E, Myerson MS. The painful total ankle arthroplasty: a diagnostic and treatment algorithm. Bone Jt J. 2017; 99-B(1):5–11.
8. Jasper LL, Jones CA, Mollins J, Pohar SL, Beaupre LA. Risk factors for revision of total knee arthroplasty: a scoping review. BMC Musculoskeletal Disord. 2016; 17(1):182.
9. Ren K, Dusad A, Yuan F, Yuan H, Purdue PE, Fehringer EV, Garvin KL, Goldring SR, Wang D. Macromolecular prodrug of dexamethasone prevents particle-induced peri-implant osteolysis with reduced systemic side effects. J Controlled Release. 2014; 175:1–9.
10. Ren K, Purdue PE, Burton L, Quan L-d, Fehringer EV, Thiele GM, Goldring SR, Wang D. Early Detection and Treatment of Wear Particle-Induced Inflammation and Bone Loss in a Mouse

Calvarial Osteolysis Model Using HPMA Copolymer Conjugates. Mol Pharmaceutics. 2011; 8(4): 1043–1051.

11. Gao SQ, Lu ZR, Kopečková P, Kopeček J. Biodistribution and pharmacokinetics of colon-specific HPMA copolymer–9-aminocamptothecin conjugate in mice. J Controlled Release. 2007; 117(2): 179–185.
12. Pan H, Sima M, Kopečková P, Wu K, Gao S, Liu J, Wang D, Miller SC, Kopeček J. Biodistribution and Pharmacokinetic Studies of Bone-Targeting N-(2-Hydroxypropyl)methacrylamide Copolymer–Alendronate Conjugates. Mol Pharmaceutics. 2008; 5(4):548–558.
13. Quan, L-d, Yuan, F., Liu, X-m, Huang, J-g, Alnouti, Y., Wang, D. Pharmacokinetic and Biodistribution Studies of N-(2-Hydroxypropyl)methacrylamide Copolymer-Dexamethasone Conjugates in Adjuvant-Induced Arthritis Rat Model. Mol Pharmaceutics. 2010; 7(4):1041–1049.
14. Wang D, Sima M, Mosley RL, Davda JP, Tietze N, Miller SC, Gwilt PR, Kopečková P, Kopeček J. Pharmacokinetic and Biodistribution Studies of a Bone-Targeting Drug Delivery System Based on N-(2-Hydroxypropyl)methacrylamide Copolymers. Mol Pharmaceutics. 2006; 3(6):717–725.
15. Lai JT, Filla D, Shea R. Functional Polymers from Novel Carboxyl-Terminated Trithiocarbonates as Highly Efficient RAFT Agents. Macromolecules. 2002; 35(18):6754–6756.
16. Liu XM, Quan LD, Tian J, Alnouti Y, Fu K, Thiele GM, Wang D. Synthesis and Evaluation of a Well-defined HPMA Copolymer–Dexamethasone Conjugate for Effective Treatment of Rheumatoid Arthritis. Pharm Res. 2008; 25(12):2910–2919. [PubMed: 18649124]
17. Ren K, Dusad A, Zhang Y, Purdue PE, Fehringer EV, Garvin KL, Goldring SR, Wang D. Early Diagnosis of Orthopedic Implant Failure Using Macromolecular Imaging Agents. Pharm Res. 2014; 31(8):2086–2094. [PubMed: 24590878]
18. Yuan F, Nelson RK, Tabor DE, Zhang Y, Akhter MP, Gould KA, Wang D. Dexamethasone prodrug treatment prevents nephritis in lupus-prone (NZB × NZW)F1 mice without causing systemic side effects. Arthritis Rheum. 2012; 64(12):4029–4039. [PubMed: 22886616]
19. Ren K, Yuan H, Zhang Y, Wei X, Wang D. Macromolecular glucocorticoid prodrug improves the treatment of dextran sulfate sodium-induced mice ulcerative colitis. Clin Immunol. 2015; 160(1): 71–81. [PubMed: 25869296]
20. Purdue PE, Levin AS, Ren K, Sculco TP, Wang D, Goldring SR. Development of Polymeric Nanocarrier System for Early Detection and Targeted Therapeutic Treatment of Peri-Implant Osteolysis. HSS J. 2013; 9(1):79–85. [PubMed: 24426848]
21. Maeda H. The enhanced permeability and retention (EPR) effect in tumor vasculature: the key role of tumor-selective macromolecular drug targeting. Adv Enzyme Regul. 2001; 41(1):189–207. [PubMed: 11384745]
22. Zhang Y, Jia Z, Yuan H, Dusad A, Ren K, Wei X, Fehringer EV, Purdue PE, Daluiski A, Goldring SR, Wang D. The Evaluation of Therapeutic Efficacy and Safety Profile of Simvastatin Prodrug Micelles in a Closed Fracture Mouse Model. Pharm Res. 2016; 33(8):1959–1971. [PubMed: 27164897]
23. Jia Z, Zhang Y, Chen YH, Dusad A, Yuan H, Ren K, Li F, Fehringer EV, Purdue PE, Goldring SR, Daluiski A, Wang D. Simvastatin prodrug micelles target fracture and improve healing. J Controlled Release. 2015; 200:23–34.
24. Yuan F, Quan L-d, Cui L, Goldring SR, Wang D. Development of macromolecular prodrug for rheumatoid arthritis. Adv Drug Delivery Rev. 2012; 64(12):1205–1219.
25. Allmeroth M, Moderegger D, Gündel D, Buchholz HG, Mohr N, Koynov K, Rösch F, Thews O, Zentel R. PEGylation of HPMA-based block copolymers enhances tumor accumulation in vivo: A quantitative study using radiolabeling and positron emission tomography. J Controlled Release. 2013; 172(1):77–85.
26. Etrych T, Šubr V, Strohalm J, Šírová M, Říhová B, Ulbrich K. HPMA copolymer-doxorubicin conjugates: The effects of molecular weight and architecture on biodistribution and in vivo activity. J Controlled Release. 2012; 164(3):346–354.
27. Allmeroth M, Moderegger D, Biesalski B, Koynov K, Rösch F, Thews O, Zentel R. Modifying the Body Distribution of HPMA-Based Copolymers by Molecular Weight and Aggregate Formation. Biomacromolecules. 2011; 12(7):2841–2849. [PubMed: 21692523]

28. Quan L, Zhang Y, Dusad A, Ren K, Purdue PE, Goldring SR, Wang D. The Evaluation of the Therapeutic Efficacy and Side Effects of a Macromolecular Dexamethasone Prodrug in the Collagen-Induced Arthritis Mouse Model. Pharm Res. 2016; 33(1):186–193. [PubMed: 26286188]

29. Yu Q, Wei Z, Shi J, Guan S, Du N, Shen T, Tang H, Jia B, Wang F, Gan Z. Polymer–Doxorubicin Conjugate Micelles Based on Poly(ethylene glycol) and Poly(N-(2-hydroxypropyl) methacrylamide): Effect of Negative Charge and Molecular Weight on Biodistribution and Blood Clearance. Biomacromolecules. 2015; 16(9):2645–2655. [PubMed: 26133354]

30. Kettiger H, Schipanski A, Wick P, Huwyler J. Engineered nanomaterial uptake and tissue distribution: from cell to organism. Int J Nanomed. 2013; 8:3255–3269.

31. Drobník J, Rypáček F. Soluble synthetic polymers in biological systems. Adv Polym Sci. 1984; 57:1–50.

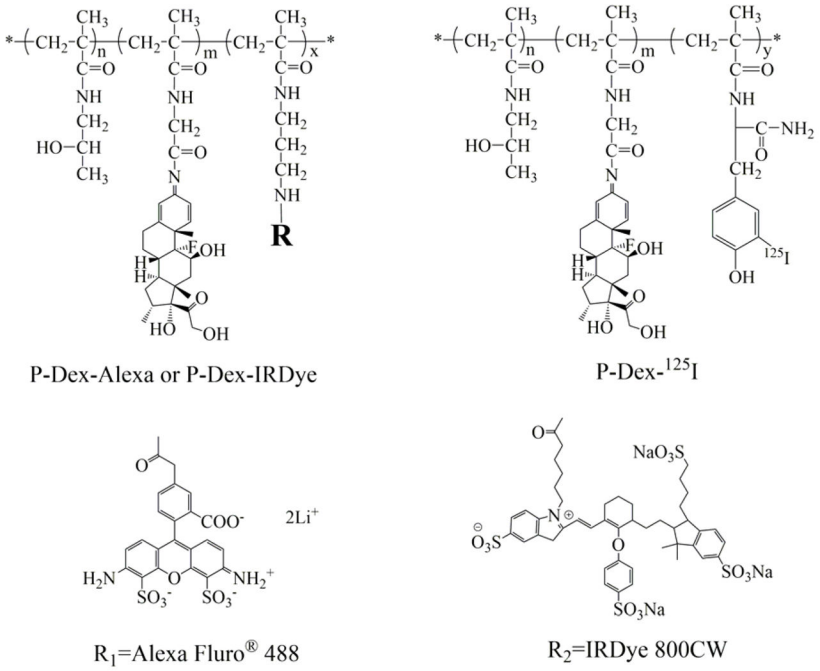

Figure 1.
The general structure of the HPMA copolymer conjugates.

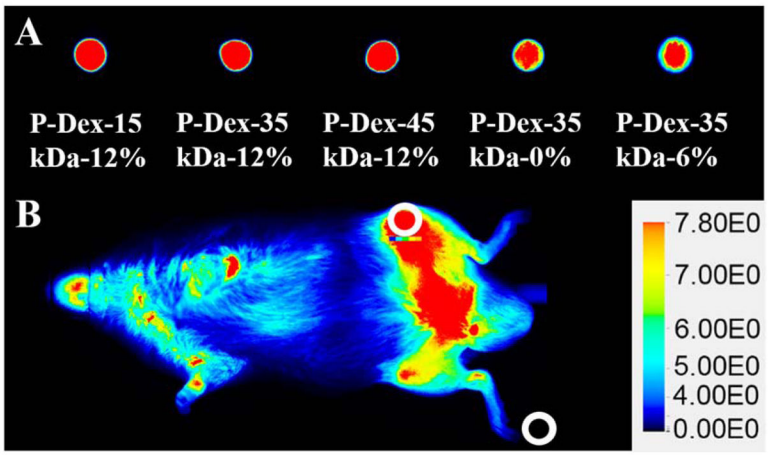

Figure 2.

The near infrared imaging analytical method for mice with systemically administered P-Dex-IRDye conjugates. A. Images of conjugate solution drops (20 μL, 3 mg/mL). The percentage represents the Dex content in each polymer conjugate tested. B. The circled areas identify representative regions of interest (ROI) and background selected for analyses.

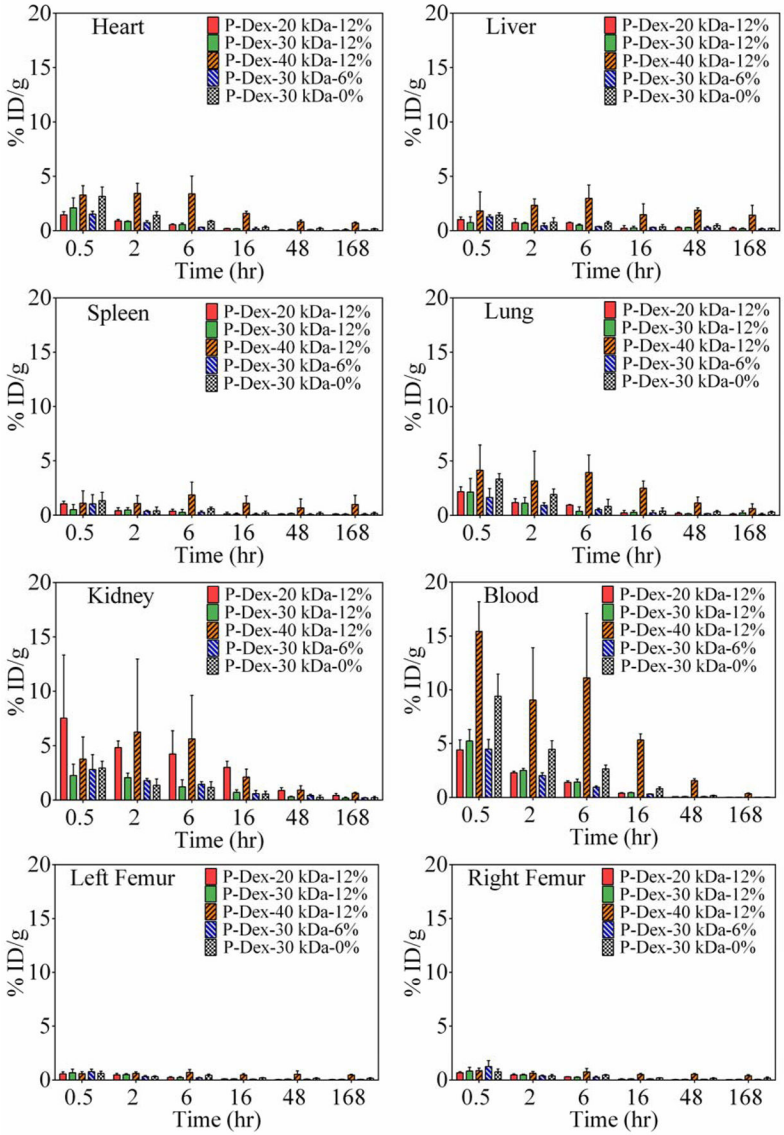

Figure 3.

The pharmacokinetics profiles of HPMA copolymer conjugates with different molecular weights and Dex contents in blood and major organs/tissues over the time course of 7 days post i.v. administration. n=5.

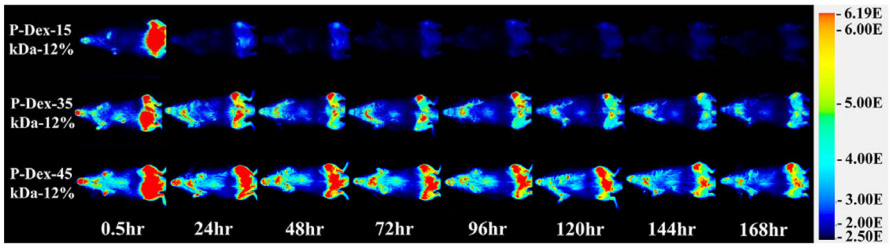

Figure 4.

Representative NIR optical images of mice with femur implants challenged with PMMA particles on left femur and PBS on the contralateral side. Images were obtained 0.5, 24, 48, 72, 96, 120, 144 and 168 hr after one intravenous injection of P–Dex-IRDye conjugates (Dex content ~12 wt%, with different MW). Pseudo color-coded signal intensity reflects the level of polymers within the mice. The signal intensity was normalized using the same intensity scale for each image.

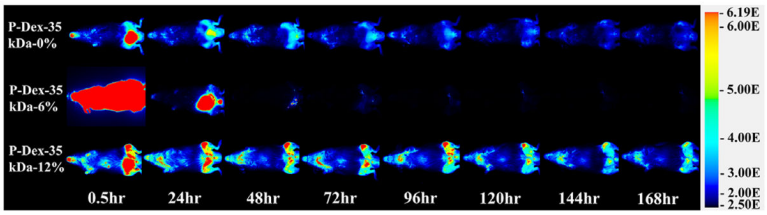

Figure 5.

Representative NIR optical images of mice with femur implants challenged with PMMA particles on left femur and PBS on the contralateral side. Images were obtained 0.5, 24, 48, 72, 96, 120, 144 and 168 hr after one intravenous injection of P-Dex (MW ~ 35 kDa, with different Dex content) at designed time points. Pseudo color-coded signal intensity reflects the level of polymers within the mice. The signal intensity was normalized using the same intensity scale for each image.

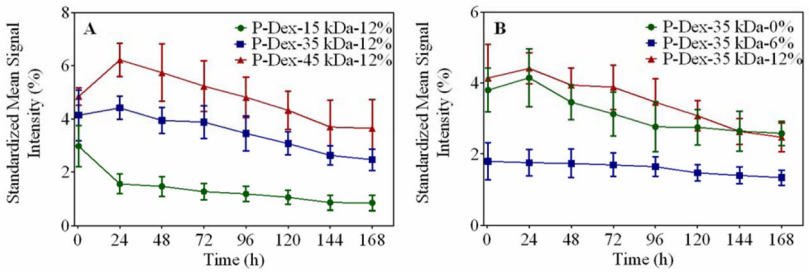

Figure 6.

Semi-quantitative analysis of the peri-implant NIR fluorescent signals from live animal optical imaging study.

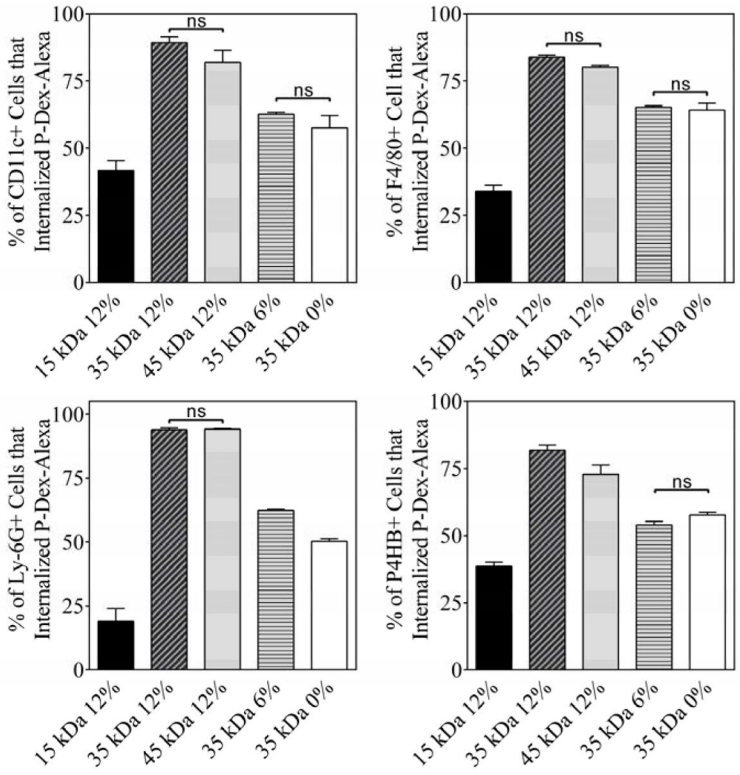

Figure 7.

The percentage of different cell phenotypes isolated from peri-implant region that internalized different HPMA copolymers-Dex conjugate. Except for those noted as not significant (ns, $P > 0.05$), all the other paired group comparisons are statistically significant ($P < 0.05$).

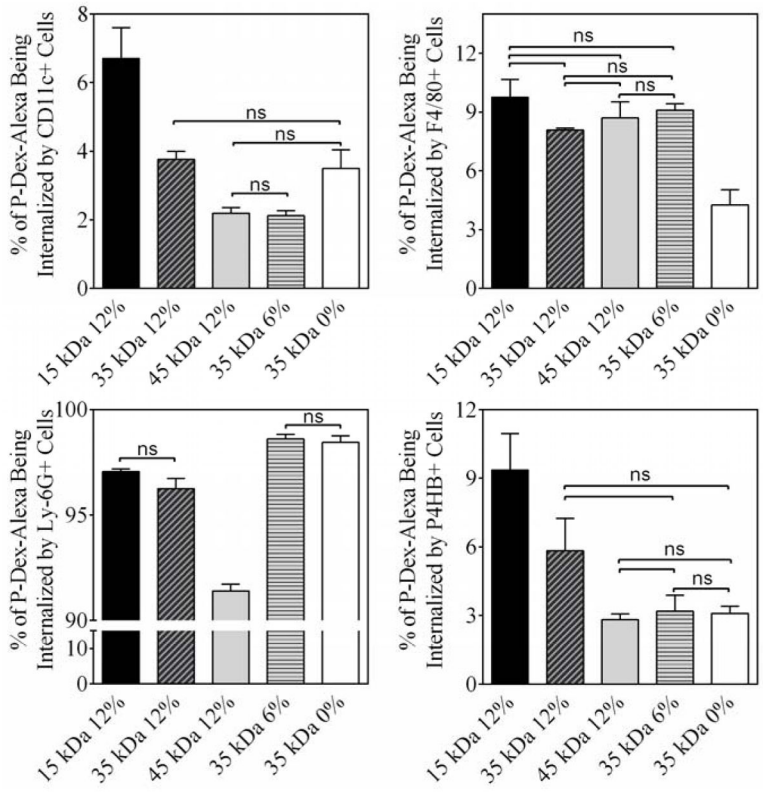

Figure 8.

The percentage of P-Dex-Alexa internalized by different cell phenotypes isolated from peri-implant region. Except for those noted as not significant (ns, $P > 0.05$), all the other paired group comparisons are statistically significant ($P < 0.05$).

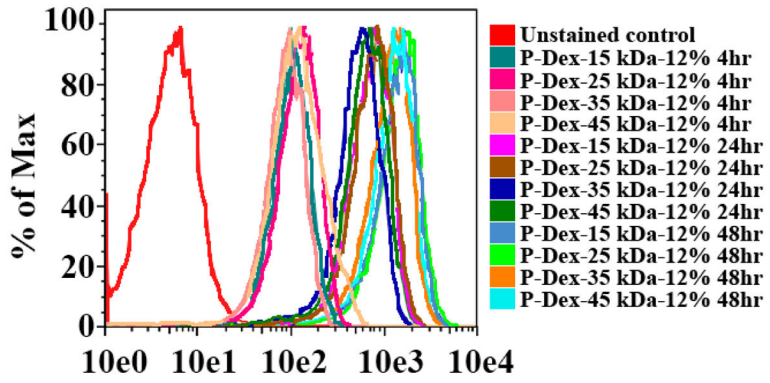

Figure 9.

In vitro flow cytometry analysis of murine BMM internalization of P-Dex with different molecular weight (Dex content ~12 wt%, labeled with Alexa Fluor® 488)

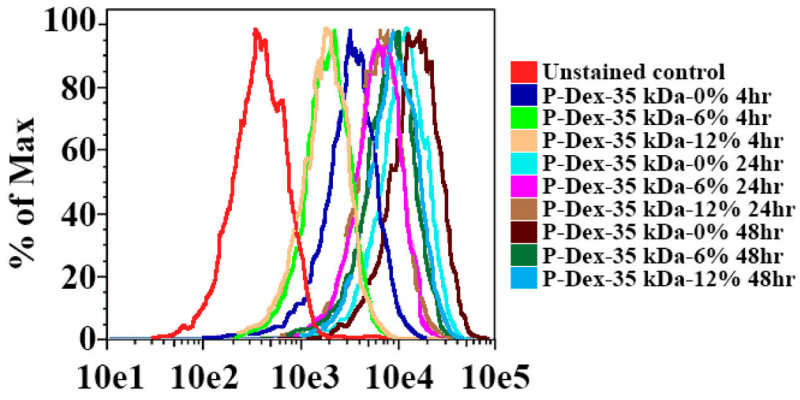

Figure 10.

In vitro flow cytometry analysis of murine BMM internalization of P-Dex with different Dex content (molecular weight ~ 35 kDa, labeled with Alexa Fluor® 488)

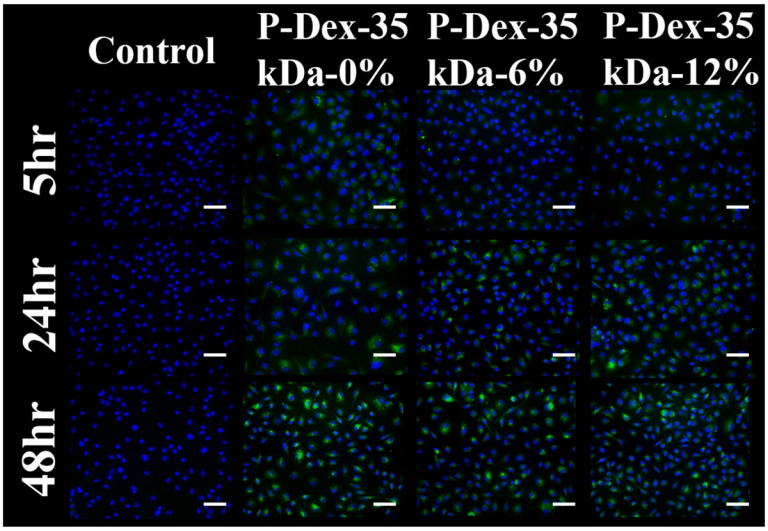

Figure 11.

In vitro fluorescence microscope analysis of murine BMM internalization of P–Dex (MW ~ 35 kDa, with different Dex content), 20×, scale bar = 50 μm.

Table 1

The characterization of HPMA copolymer conjugates labeled with ^{125}I. M_w: weight average molecular weight; PDI: polydispersity index.

Polymerconjugates	M_w (× 10^3 g/mol)	PDI	Dex content (μmol/g) (mol%)	Radioactivity (μCi/g)
P-Dex-20 kDa-12%	20.5	1.11	283.09 ± 35.16 (4.7)	138.8
P-Dex-30 kDa-12%	30.7	1.18	346.28 ± 10.70 (5.9)	394.8
P-Dex-40 kDa-12%	39.1	1.21	341.94 ± 25.98 (5.9)	354.8
P-Dex-30 kDa-6%	35.3	1.17	170.46 ± 22.42 (2.7)	200.4
P-Dex-30 kDa-0%	30.8	1.06	0 (0)	180.8

Table 2

The characterization of HPMA copolymer conjugates labeled with fluorescent probes. M_w: weight average molecular weight; PDI: polydispersity index: Dexamethasone content; [Alexa-488]: Alexa Fluor® 488 content; [IRDye-800CW]: IRDye 800CW content

Polymer conjugates	M_w (×10^3 g/mol)	PDI	Dex Content (μmol/g) (mol %)	[Alexa 488] (μmol/g) (mol%)	[IRDye 800CW] (μmol/g) (mol%)
P-Dex-15 kDa-12%	15.9	1.35	306.55 ± 27.24 (5.1)	10.89 ± 0.15 (0.18)	6.20 ± 0.14 (0.10)
P-Dex-25 kDa-12%	27.5	1.4	300.13 ± 11.23 (5.0)	13.82 ± 0.27 (0.23)	6.08 ± 0.31 (0.10)
P-Dex-35 kDa-12%	35.3	1.49	356.34 ± 39.55 (6.0)	10.25 ± 0.20 (0.17)	7.89 ± 0.04 (0.13)
P-Dex-45 kDa-12%	45.3	1.34	315.32 ± 18.40 (5.3)	12.63 ± 1.28 (0.21)	7.55 ± 0.14 (0.13)
P-Dex-35 kDa-6%	35.7	1.29	168.86 ± 20.33 (2.7)	11.83 ± 0.38 (0.19)	7.54 ± 0.10 (0.12)
P-Dex-35 kDa-0%	36.0	1.45	0 (0)	13.50 ± 0.30 (0.23)	7.83 ± 0.11 (0.13)

Table 3

The pharmacokinetic (PK) parameters of different HPMA copolymer conjugates after systemic administration. $t_{1/2}$, the half-life associated with the elimination phase; CL, total body clearance; V_{ss}, volume of distribution in steady state; AUC, area under a concentration of analyte vs time curve.

Parameters (unit)	P-Dex-20 kDa-12%	P-Dex-30 kDa-12%	P-Dex-40 kDa-12%	P-Dex-30 kDa-6%	P-Dex-30 kDa-0%
$t_{1/2}$ (hr)	27.4 ± 5.9	22.3 ± 6.6	35.8 ± 3.7	23.9 ± 3.5	24.3 ± 4.7
Cl (mL/hr/kg)	316.9 ± 19.1	115.7 ± 10.6	12.5 ± 0.9	238.6 ± 11.6	73.9 ± 3.8
V_{ss}(mL/kg)	6,473.5 ± 301.6	1,850.6 ± 274.2	516.4 ± 77.7	4,225.1 ± 516.2	1,332.2 ± 154.3
$AUC_{0-\infty}$ (blood) (hr* count/gm)	376,071.8 ± 22102.0	1,057,256.4 ± 103135.1	10,134,744.0 ± 732647.0	520,626.4 ± 24637.4	1,682,399.0 ± 86933.0
AUC (% extrapolation)	1.1 ± 0.5	1.3 ± 1.5	4.2 ± 1.4	0.6 ± 0.3	0.7 ± 0.4
$AUC_{left\ femur}/AUC_{bood}$	0.34	0.38	0.23	0.43	0.39
$AUC_{right\ femur}/AUC_{bood}$	0.33	0.35	0.23	0.49	0.41
AUC_{heart}/AUC_{bood}	0.67	0.71	0.49	0.74	0.64
AUC_{liver}/AUC_{bood}	1.43	1.1	0.8	1.36	0.84
AUC_{spleen}/AUC_{bood}	0.64	0.52	0.42	0.45	0.43
AUC_{lungs}/AUC_{bood}	1.1	0.92	0.60	0.98	0.85
AUC_{kidney}/AUC_{bood}	6.02	1.6	0.57	2.32	0.77
$MRT_{0-\infty}$ (blood) (hr)	20.4 ± 0.6	16.1 ± 2.8	41.4 ± 5.9	17.7 ± 2.2	18.0 ± 1.3
$MRT_{left\ femur}/MRT_{bood}$	2.94	3.57	2.58	3.74	4.34
$MRT_{right\ femur}/MRT_{bood}$	2.97	3.54	2.44	3.43	4.33
MRT_{heart}/MRT_{bood}	2.64	3.36	2.03	3.29	3.30
MRT_{liver}/MRT_{bood}	4.06	4.09	2.38	3.83	3.68
MRT_{spleen}/MRT_{bood}	4.54	4.21	2.43	3.37	3.83
MRT_{lungs}/MRT_{bood}	2.88	4.29	1.70	3.08	3.85
MRT_{kidney}/MRT_{bood}	2.42	3.06	1.70	2.94	2.93

Table 4

The percentage of different cell phenotypes that internalized P-Dex-Alexa at the peri-implant region.

Polymer	P-Dex-15 kDa-12%	P-Dex-35 kDa-12%	P-Dex-45 kDa-12%	P-Dex-35 kDa-6%	P-Dex-35 kDa-0%
CD11c+	41.67	89.28	81.98	62.63	57.53
F4/80+	34.01	83.85	80.09	65.22	64.19
Ly6G+	18.99	93.94	94.16	62.38	50.20
P4HB	38.61	81.75	72.79	54.008	57.77

Table 5

The percentage of P-Dex-Alexa being sequestered by different cell phenotypes at the peri-implant region.

Polymer	P-Dex-15 kDa-12%	P-Dex-35 kDa-12%	P-Dex-45 kDa-12%	P-Dex-35 kDa-6%	P-Dex-35 kDa-0%
CD11c+	6.70	3.76	2.19	2.12	3.50
F4/80+	9.75	8.07	8.70	9.10	4.26
Ly6G+	97.07	96.26	91.40	98.61	98.45
P4HB	9.37	5.83	2.81	3.18	3.09

Table 6

Dynamic light scattering (DLS) analysis of copolymers at a concentration of 5 mg/mL. Z-Ave: Z-Average size (diameter.nm); PDI: Polydispersity index.

Sample Name	P-Dex-15 kDa-12%	P-Dex-35 kDa-12%	P-Dex-45 kDa-12%	P-Dex-35 kDa-6%	P-Dex-35 kDa-0%
Z-Ave (d.nm)	6.643	7.673	8.552	163.9	6.828
PDI	0.237	0.318	0.209	0.481	0.174

Table 7

Dynamic light scattering (DLS) analysis P-Dex-35 kDa-6% at different concentration. Z-Ave: Z-Average size (diameter.nm); PDI: Polydispersity index.

Concentration (mg/mL)	5	37.5	150
Z-Ave (d.nm)	163.9	282.9	313.6
PDI	0.481	0.769	1